Observation of χ_{cJ} decays to ΛΛ[over ¯]π^{+}π^{-}

M. Ablikim *et al.* (BESIII Collaboration)

Observation of χ_{cJ} Decays to $\Lambda\bar{\Lambda}\pi^+\pi^-$

M. Ablikim[1], M. N. Achasov[5], D. J. Ambrose[39], F. F. An[1], Q. An[40], Z. H. An[1], J. Z. Bai[1],

Y. Ban[27], J. Becker[2], M. Bertani[18A], J. M. Bian[38], E. Boger[20,a], O. Bondarenko[21], I. Boyko[20],

R. A. Briere[3], V. Bytev[20], X. Cai[1], O. Cakir[35A], A. Calcaterra[18A], G. F. Cao[1], S. A. Cetin[35B],

J. F. Chang[1], G. Chelkov[20,a], G. Chen[1], H. S. Chen[1], J. C. Chen[1], M. L. Chen[1], S. J. Chen[25],

Y. B. Chen[1], H. P. Cheng[14], Y. P. Chu[1], D. Cronin-Hennessy[38], H. L. Dai[1], J. P. Dai[1],

D. Dedovich[20], Z. Y. Deng[1], A. Denig[19], I. Denysenko[20,b], M. Destefanis[43A,43C], W. M. Ding[29],

Y. Ding[23], L. Y. Dong[1], M. Y. Dong[1], S. X. Du[46], J. Fang[1], S. S. Fang[1], L. Fava[43B,43C],

F. Feldbauer[2], C. Q. Feng[40], R. B. Ferroli[18A], C. D. Fu[1], J. L. Fu[25], Y. Gao[34], C. Geng[40],

K. Goetzen[7], W. X. Gong[1], W. Gradl[19], M. Greco[43A,43C], M. H. Gu[1], Y. T. Gu[9], Y. H. Guan[6],

A. Q. Guo[26], L. B. Guo[24], Y. P. Guo[26], Y. L. Han[1], F. A. Harris[37], K. L. He[1], M. He[1],

Z. Y. He[26], T. Held[2], Y. K. Heng[1], Z. L. Hou[1], H. M. Hu[1], J. F. Hu[6], T. Hu[1], G. M. Huang[15],

J. S. Huang[12], X. T. Huang[29], Y. P. Huang[1], T. Hussain[42], C. S. Ji[40], Q. Ji[1], X. B. Ji[1],

X. L. Ji[1], L. L. Jiang[1], X. S. Jiang[1], J. B. Jiao[29], Z. Jiao[14], D. P. Jin[1], S. Jin[1], F. F. Jing[34],

N. Kalantar-Nayestanaki[21], M. Kavatsyuk[21], W. Kuehn[36], W. Lai[1], J. S. Lange[36], C. H. Li[1],

Cheng Li[40], Cui Li[40], D. M. Li[46], F. Li[1], G. Li[1], H. B. Li[1], J. C. Li[1], K. Li[10], Lei Li[1], Q. J. Li[1],

S. L. Li[1], W. D. Li[1], W. G. Li[1], X. L. Li[29], X. N. Li[1], X. Q. Li[26], X. R. Li[28], Z. B. Li[33],

H. Liang[40], Y. F. Liang[31], Y. T. Liang[36], G. R. Liao[34], X. T. Liao[1], B. J. Liu[1], C. L. Liu[3],

C. X. Liu[1], C. Y. Liu[1], F. H. Liu[30], Fang Liu[1], Feng Liu[15], H. Liu[1], H. B. Liu[6], H. H. Liu[13],

H. M. Liu[1], H. W. Liu[1], J. P. Liu[44], K. Y. Liu[23], Kai Liu[6], P. L. Liu[29], Q. Liu[6], S. B. Liu[40],

X. Liu[22], X. H. Liu[1], Y. B. Liu[26], Z. A. Liu[1], Zhiqiang Liu[1], Zhiqing Liu[1], H. Loehner[21],

G. R. Lu[12], H. J. Lu[14], J. G. Lu[1], Q. W. Lu[30], X. R. Lu[6], Y. P. Lu[1], C. L. Luo[24], M. X. Luo[45],

T. Luo[37], X. L. Luo[1], M. Lv[1], C. L. Ma[6], F. C. Ma[23], H. L. Ma[1], Q. M. Ma[1], S. Ma[1], T. Ma[1],

X. Y. Ma[1], Y. Ma[11], F. E. Maas[11], M. Maggiora[43A,43C], Q. A. Malik[42], Y. J. Mao[27], Z. P. Mao[1],

J. G. Messchendorp[21], J. Min[1], T. J. Min[1], R. E. Mitchell[17], X. H. Mo[1], C. Morales

Morales[11], C. Motzko[2], N. Yu. Muchnoi[5], H. Muramatsu[39], Y. Nefedov[20], C. Nicholson[6],

I. B. Nikolaev[5], Z. Ning[1], S. L. Olsen[28], Q. Ouyang[1], S. Pacetti[18B], J. W. Park[28], M. Pelizaeus[37],

H. P. Peng[40], K. Peters[7], J. L. Ping[24], R. G. Ping[1], R. Poling[38], E. Prencipe[19], M. Qi[25],

S. Qian[1], C. F. Qiao[6], X. S. Qin[1], Y. Qin[27], Z. H. Qin[1], J. F. Qiu[1], K. H. Rashid[42], G. Rong[1],

X. D. Ruan[9], A. Sarantsev[20,c], B. D. Schaefer[17], J. Schulze[2], M. Shao[40], C. P. Shen[37,d],

X. Y. Shen[1], H. Y. Sheng[1], M. R. Shepherd[17], X. Y. Song[1], S. Spataro[43A,43C], B. Spruck[36],

D. H. Sun[1], G. X. Sun[1], J. F. Sun[12], S. S. Sun[1], Y. J. Sun[40], Y. Z. Sun[1], Z. J. Sun[1], Z. T. Sun[40],

C. J. Tang[31], X. Tang[1], I. Tapan[35C], E. H. Thorndike[39], D. Toth[38], M. Ullrich[36], G. S. Varner[37],

B. Wang[9], B. Q. Wang[27], K. Wang[1], L. L. Wang[4], L. S. Wang[1], M. Wang[29], P. Wang[1],

P. L. Wang[1], Q. Wang[1], Q. J. Wang[1], S. G. Wang[27], X. L. Wang[40], Y. D. Wang[40], Y. F. Wang[1],

Y. Q. Wang[29], Z. Wang[1], Z. G. Wang[1], Z. Y. Wang[1], D. H. Wei[8], P. Weidenkaff[19],

Q. G. Wen[40], S. P. Wen[1], M. Werner[36], U. Wiedner[2], L. H. Wu[1], N. Wu[1], S. X. Wu[40],

W. Wu[26], Z. Wu[1], L. G. Xia[34], Z. J. Xiao[24], Y. G. Xie[1], Q. L. Xiu[1], G. F. Xu[1], G. M. Xu[27],

H. Xu[1], Q. J. Xu[10], X. P. Xu[32], Z. R. Xu[40], F. Xue[15], Z. Xue[1], L. Yan[40], W. B. Yan[40],

Y. H. Yan[16], H. X. Yang[1], Y. Yang[15], Y. X. Yang[8], H. Ye[1], M. Ye[1], M. H. Ye[4], B. X. Yu[1],

C. X. Yu[26], J. S. Yu[22], S. P. Yu[29], C. Z. Yuan[1], Y. Yuan[1], A. A. Zafar[42], A. Zallo[18A], Y. Zeng[16],

B. X. Zhang[1], B. Y. Zhang[1], C. C. Zhang[1], D. H. Zhang[1], H. H. Zhang[33], H. Y. Zhang[1],

J. Q. Zhang[1], J. W. Zhang[1], J. Y. Zhang[1], J. Z. Zhang[1], S. H. Zhang[1], X. J. Zhang[1],

X. Y. Zhang[29], Y. Zhang[1], Y. H. Zhang[1], Y. S. Zhang[9], Z. P. Zhang[40], Z. Y. Zhang[44], G. Zhao[1],

H. S. Zhao[1], J. W. Zhao[1], K. X. Zhao[24], Lei Zhao[40], Ling Zhao[1], M. G. Zhao[26], Q. Zhao[1],

S. J. Zhao[46], T. C. Zhao[1], X. H. Zhao[25], Y. B. Zhao[1], Z. G. Zhao[40], A. Zhemchugov[20,a],

B. Zheng[41], J. P. Zheng[1], Y. H. Zheng[6], B. Zhong[1], J. Zhong[2], L. Zhou[1], X. K. Zhou[6],

X. R. Zhou[40], C. Zhu[1], K. Zhu[1], K. J. Zhu[1], S. H. Zhu[1], X. L. Zhu[34], X. W. Zhu[1],

Y. C. Zhu[40], Y. M. Zhu[26], Y. S. Zhu[1], Z. A. Zhu[1], J. Zhuang[1], B. S. Zou[1], J. H. Zou[1]

(BESIII Collaboration)

[1] *Institute of High Energy Physics, Beijing 100049, P. R. China*

[2] *Bochum Ruhr-University, 44780 Bochum, Germany*

[3] *Carnegie Mellon University, Pittsburgh, PA 15213, USA*

[4] *China Center of Advanced Science and Technology, Beijing 100190, P. R. China*

[5] *G.I. Budker Institute of Nuclear Physics SB RAS (BINP), Novosibirsk 630090, Russia*

[6] *Graduate University of Chinese Academy of Sciences, Beijing 100049, P. R. China*

[7] *GSI Helmholtzcentre for Heavy Ion Research GmbH, D-64291 Darmstadt, Germany*

[8] *Guangxi Normal University, Guilin 541004, P. R. China*

[9] *GuangXi University, Nanning 530004,P.R.China*

[10] *Hangzhou Normal University, Hangzhou 310036, P. R. China*

[11] *Helmholtz Institute Mainz, J.J. Becherweg 45,D 55099 Mainz,Germany*

[12] *Henan Normal University, Xinxiang 453007, P. R. China*

[13] *Henan University of Science and Technology, Luoyang 471003, P. R. China*

[14] *Huangshan College, Huangshan 245000, P. R. China*

[15] *Huazhong Normal University, Wuhan 430079, P. R. China*

[16] *Hunan University, Changsha 410082, P. R. China*

[17] *Indiana University, Bloomington, Indiana 47405, USA*

[18] *(A)INFN Laboratori Nazionali di Frascati, Frascati, Italy;*

(B)INFN and University of Perugia, I-06100, Perugia, Italy

[19] *Johannes Gutenberg University of Mainz,*

Johann-Joachim-Becher-Weg 45, 55099 Mainz, Germany

[20] *Joint Institute for Nuclear Research, 141980 Dubna, Russia*

[21] *KVI/University of Groningen, 9747 AA Groningen, The Netherlands*

[22] *Lanzhou University, Lanzhou 730000, P. R. China*

[23] *Liaoning University, Shenyang 110036, P. R. China*

[24] *Nanjing Normal University, Nanjing 210046, P. R. China*

[25] *Nanjing University, Nanjing 210093, P. R. China*

[26] *Nankai University, Tianjin 300071, P. R. China*

[27] *Peking University, Beijing 100871, P. R. China*

[28] *Seoul National University, Seoul, 151-747 Korea*

[29] *Shandong University, Jinan 250100, P. R. China*

[30] *Shanxi University, Taiyuan 030006, P. R. China*

[31] *Sichuan University, Chengdu 610064, P. R. China*

[32] *Soochow University, Suzhou 215006, China*

[33] *Sun Yat-Sen University, Guangzhou 510275, P. R. China*

[34] *Tsinghua University, Beijing 100084, P. R. China*

[35] *(A)Ankara University, Ankara, Turkey; (B)Dogus University,*

Istanbul, Turkey; (C)Uludag University, Bursa, Turkey

[36] *Universitaet Giessen, 35392 Giessen, Germany*

[37] *University of Hawaii, Honolulu, Hawaii 96822, USA*

[38] *University of Minnesota, Minneapolis, MN 55455, USA*

[39] *University of Rochester, Rochester, New York 14627, USA*

[40] *University of Science and Technology of China, Hefei 230026, P. R. China*

[41] *University of South China, Hengyang 421001, P. R. China*

[42] *University of the Punjab, Lahore-54590, Pakistan*

[43] *(A)University of Turin, Turin, Italy; (B)University of Eastern Piedmont, Alessandria, Italy; (C)INFN, Turin, Italy*

[44] *Wuhan University, Wuhan 430072, P. R. China*

[45] *Zhejiang University, Hangzhou 310027, P. R. China*

[46] *Zhengzhou University, Zhengzhou 450001, P. R. China*

[a] *also at the Moscow Institute of Physics and Technology, Moscow, Russia*

[b] *on leave from the Bogolyubov Institute for Theoretical Physics, Kiev, Ukraine*

[c] *also at the PNPI, Gatchina, Russia*

[d] *now at Nagoya University, Nagoya, Japan*

Decays of the χ_{cJ} states (J=0, 1, 2) to $\Lambda\bar{\Lambda}\pi^+\pi^-$, including processes with intermediate $\Sigma(1385)$, are studied through the $E1$ transition $\psi' \to \gamma\chi_{cJ}$ using 106 million ψ' events collected with the BESIII detector at BEPCII. This is the first observation of χ_{cJ} decays to the final state $\Lambda\bar{\Lambda}\pi^+\pi^-$. The branching ratio of the intermediate process $\chi_{cJ} \to \Sigma(1385)^\pm\bar{\Sigma}(1385)^\mp$ is also measured for the first time, and the results agree with the theoretical predictions based on the color-octet effect.

I.   INTRODUCTION

Decays of P-wave charmonium states, *e.g.*, the χ_{cJ}, cannot be well explained by the color-singlet contribution alone, although this works well in explaining the decays of S-wave charmonium, *e.g.*, the J/ψ and ψ'. In calculations of the color-octet contribution, Ref. [1] predicted branching ratios of $\chi_{cJ} \rightarrow$ baryon+anti-baryon in which the $\chi_{cJ} \rightarrow p\bar{p}$ result is consistent with experimental observation, while the $\chi_{cJ} \rightarrow \Lambda\bar{\Lambda}$ [2] result is not. The calculated branching ratios are $\mathcal{B}(\chi_{c1} \rightarrow \Lambda\bar{\Lambda}) = (3.91 \pm 0.24) \times 10^{-5}$ and $\mathcal{B}(\chi_{c2} \rightarrow \Lambda\bar{\Lambda}) = (3.49 \pm 0.20) \times 10^{-5}$, while the experimental results are $(11.8 \pm 1.9) \times 10^{-5}$ and $(18.6 \pm 2.7) \times 10^{-5}$, respectively. In addition to $\Lambda\bar{\Lambda}$, reference [1] also calculated the branching ratios of $\chi_{c1} \rightarrow \Sigma(1385)\bar{\Sigma}(1385)$ and $\chi_{c2} \rightarrow \Sigma(1385)\bar{\Sigma}(1385)$ to be $(2.15 \pm 0.12) \times 10^{-5}$ and $(3.61 \pm 0.20) \times 10^{-5}$, respectively, but there are no previous experimental results on these decay channels. Therefore, it is meaningful to test these predictions experimentally. In addition, due to the helicity selection rule, the decay of χ_{c0} into baryon-antibaryon is expected to be suppressed [3].

In this paper, we report measurements of $\chi_{cJ} \rightarrow \Lambda\bar{\Lambda}\pi^+\pi^-$ ($J = 0, 1, 2$) (including the intermediate $\Sigma(1385)$ resonance), $\chi_{cJ} \rightarrow \Sigma(1385)^{\pm}\bar{\Lambda}\pi^{\mp} + c.c.$, and $\chi_{cJ} \rightarrow \Sigma(1385)^{\pm}\bar{\Sigma}(1385)^{\mp}$ through the $E1$ transition $\psi' \rightarrow \gamma\chi_{cJ}$, where $\Sigma(1385)^{\pm} \rightarrow \Lambda\pi^{\pm}$ and $\Lambda \rightarrow p\pi^-$. This work is based on a 106 million ψ' event sample collected with the BESIII detector at the Beijing Electron-Positron Collider II (BEPCII) [4]. Continuum data taken at the center of mass energy $\sqrt{s} = 3.65\,\text{GeV}$, with an integrated luminosity of $42.9\,\text{pb}^{-1}$, is used to study non-ψ' decay background.

II.   THE BESIII DETECTOR

BEPCII [5] is a double-ring, multi-bunch e^+e^- collider with collision energies ranging from $2.0\,\text{GeV}$ to $4.6\,\text{GeV}$. The BESIII detector [5] is a general-purpose spectrometer with 93% coverage of full solid angle. From the interaction point outwards, BESIII is composed of the following: a main drift chamber consisting of 43 layers of drift cells with a space resolution of about $135\,\mu\text{m}$ and momentum resolution of about 0.5% at $1\,\text{GeV/c}$; a time-of-flight counter, which is comprised of two layers of scintillator with time resolution of $80\,\text{ps}$ in the barrel part and one layer with time resolution of $110\,\text{ps}$ in the end-cap part; an electromagnetic

calorimeter (EMC), which is comprised of 6240 CsI(Tl) crystals, with energy resolution of 2.5% in the barrel and 5.0% in the end-cap for a $1\,\mathrm{GeV}$ photon, and position resolution of $6\,\mathrm{mm}$ in the barrel and $9\,\mathrm{mm}$ in the end-cap; a super-conducting solenoid magnet, which can provide a $1\,\mathrm{T}$ magnetic field parallel to the beam direction; and a muon counter, which is made of $1000\,\mathrm{m}^2$ resistive-plate-chambers sandwiched in iron absorbers.

III.   MONTE-CARLO SIMULATION

For evaluation of the detection efficiency and understanding backgrounds, a Monte-Carlo (MC) simulation framework for BESIII was developed. A GEANT4-based MC simulation program, BOOST, is designed to simulate the interaction of particles in the spectrometer and the responses of the detector. For the generation of charmonium states, $e.g.$, ψ', an event generator, KKMC [6, 7], is employed, which handles the initial state radiative correction and the beam energy spread. For simulation of the resonant decay, BesEvtGen, based on EvtGen [8, 9], is used to realize well-measured processes, while LundCharm [8] is used for the unknown possible processes.

In the MC simulations for the processes presented here, $\psi' \to \gamma\chi_{cJ}$ is assumed to be a pure $E1$ transition, and the polar angle, θ, follows a distribution of the form $1 + \alpha\cos^2\theta$ with $\alpha = 1$, $-1/3$, and $1/13$ for $J = 0$, 1 and 2, respectively [10]. Momenta in the decay of $\chi_{cJ} \to \Sigma(1385)^\pm\bar{\Sigma}(1385)^\mp$, $\chi_{cJ} \to \Sigma(1385)^\pm\bar{\Lambda}\pi^\mp(c.c.)$ and $\chi_{cJ} \to \Lambda\bar{\Lambda}\pi^+\pi^-$ are uniformly distributed in phase space. For the decay mode $\chi_{cJ} \to \Sigma(1385)^\pm\bar{\Sigma}(1385)^\mp$, an extreme angular distribution is used to test the phase space assumption and no significant differences in efficiencies are observed. This is because, with the current level of statistics, the detection efficiencies of the final states are determined mainly by the detection of the $E1$ photons, and the angular distributions of the hadrons in the subsequent decays are not dependent on their MC decay models.

IV.   EVENT SELECTION

The candidate events for the decay modes $\psi' \to \gamma\chi_{cJ} \to \gamma\Lambda\bar{\Lambda}\pi^+\pi^-$, with $\Lambda \to p\pi$, were chosen with the following selection criteria:

(1) Charged tracks, *i.e.*, candidates for $\pi^\pm$, p and $\bar{p}$, must satisfy $|\cos\theta| \leq 0.93$, where θ is the polar angle with respect to the beam direction. Particle identification is not used.

(2) The charged tracks not assigned to any $\Lambda(\bar{\Lambda})$ decay candidates must have their point of closest approach to the interaction point within $10\,\mathrm{cm}$ along the beam direction and $1\,\mathrm{cm}$ in the perpendicular plane.

(3) A common vertex constraint is applied to each pair of charged tracks assumed to decay from $\Lambda/\bar{\Lambda}$ *i.e.*, $p\pi^-$ and $\bar{p}\pi^+$, and the production points of $\Lambda/\bar{\Lambda}$ candidates are constrained to the interaction point.

(4) A photon candidate is a shower cluster in the EMC that is not associated with any charged track and has a minimum energy deposit of $25\,\mathrm{MeV}$ in the barrel or $50\,\mathrm{MeV}$ in the end-cap.

(5) The total momentum of all final particle candidates is constrained to the initial four-momentum of the e^+e^- system in a kinematic fit. The events with $\chi^2_{4\mathrm{C}} < 80$ are retained; for an event with more than one photon candidate, only the one with the smallest $\chi^2_{4\mathrm{C}}$ is kept.

(6) Backgrounds from the decay $\psi' \to \pi^+\pi^- J/\psi$ followed by $J/\psi \to \gamma\Lambda\bar{\Lambda}$ are rejected by requiring the $\pi^+\pi^-$ recoil mass be greater than $3.108\,\mathrm{GeV}/c^2$ or less than $3.088\,\mathrm{GeV}/c^2$. The background from $\psi' \to \Sigma(1385)\bar{\Sigma}(1385)$, followed by $\Sigma(1385) \to \Sigma^0\pi$ and $\Sigma^0 \to \gamma\Lambda$, is rejected by discarding events with $\gamma\Lambda$ ($\gamma\bar{\Lambda}$) mass in the range $[1.183, 1.202]\,\mathrm{GeV}/c^2$.

V. SIGNAL ESTIMATION

The invariant mass distributions of $M_{p\pi^-}$ and $M_{\bar{p}\pi^+}$ are shown in Figs. 1(a) and (b), where the signals of Λ and $\bar{\Lambda}$ are clean. Figure 1(c) shows a scatter plot ($M_{p\pi^-}$ *versus* $M_{\bar{p}\pi^+}$). Events where $M_{p\pi^-}$ and $M_{\bar{p}\pi^+}$ fall within the box in Fig. 1(c) are used for further analysis. The invariant mass distribution of $\Lambda\bar{\Lambda}\pi^+\pi^-$, $M_{\Lambda\bar{\Lambda}\pi^+\pi^-}$, is shown in Fig. 1(d), and the three χ_{cJ} peaks are clearly observed.

The invariant masses of $\Lambda\pi^+$ and $\Lambda\pi^-$ ($\bar{\Lambda}\pi^-$ and $\bar{\Lambda}\pi^+$) are displayed in Figs. 2(a) and (c) (Figs. 2(b) and (d)), respectively. $\Sigma(1385)$ peaks are clearly seen. $\Xi^\pm$ peaks are also seen in Figs. 2(c) and (d), around its nominal mass $1.322\,\mathrm{GeV}/c^2$ [2]. The Ξ is a relatively
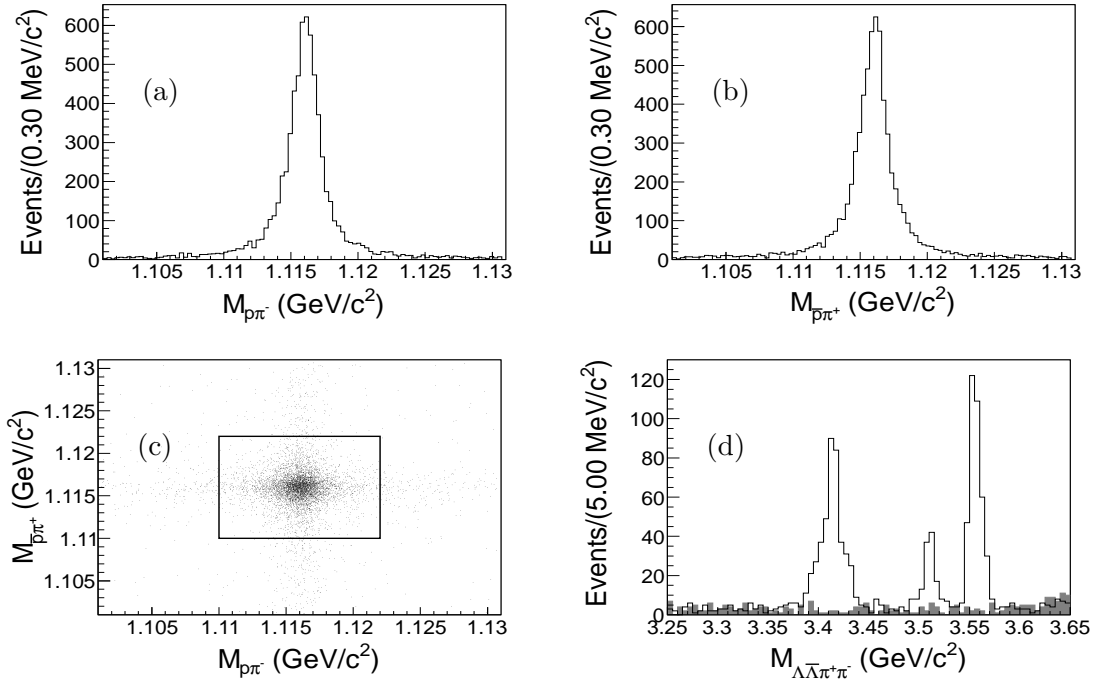
FIG. 1. (a) The invariant mass distribution $M_{p\pi^-}$ for $p\pi^-$. (b) The invariant mass distribution $M_{\bar{p}\pi^+}$ for $\bar{p}\pi^+$. (c) The scatter plot of $M_{p\pi^-}$ versus $M_{\bar{p}\pi^+}$; the box indicates the $\Lambda\bar{\Lambda}$ signal region used in this analysis. (d) The invariant mass distribution $M_{\Lambda\bar{\Lambda}\pi^+\pi^-}$ for $\Lambda\bar{\Lambda}\pi^+\pi^-$; the shaded histogram is the background estimated from the inclusive decays of the ψ' MC sample.

long-lived particle, and the selection criteria in this analysis are not optimized for a study of the Ξ. Hence, this work does not include study of processes involving Ξ. Events around the $\Xi^\pm$ peaks are rejected by requiring $M_{\Lambda\pi^-(\bar{\Lambda}\pi^+)}$ be less than $1.331\,\text{GeV}/c^2$ or greater than $1.312\,\text{GeV}/c^2$.

We divide the remaining χ_{cJ} decays into five processes: (1) $\Lambda\bar{\Lambda}\pi^+\pi^-$ (non-resonant); (2) $\Sigma(1385)^+\bar{\Lambda}\pi^-+c.c.$; (3) $\Sigma(1385)^-\bar{\Lambda}\pi^++c.c.$; (4) $\Sigma(1385)^+\bar{\Sigma}(1385)^-$; and (5) $\Sigma(1385)^-\bar{\Sigma}(1385)^+$. To study the five processes, requirements on $M_{\Lambda\pi^-(\bar{\Lambda}\pi^+)}$ are implemented as shown in Fig. 2. The areas between $1.32\,\text{GeV}/c^2$ and $1.46\,\text{GeV}/c^2$ (two solid arrows) are defined as $\Sigma(1385)$ signal regions, while the areas smaller than $1.30\,\text{GeV}/c^2$ or larger than $1.50\,\text{GeV}/c^2$ (two dashed arrows) are defined as non-$\Sigma(1385)$ regions.

Due to the broad width and the long tails of the $\Sigma(1385)$, the $\Sigma(1385)$ and non-$\Sigma(1385)$ events feed into the non-$\Sigma(1385)$ and $\Sigma(1385)$ regions. As a result, the χ_{cJ} events that decay
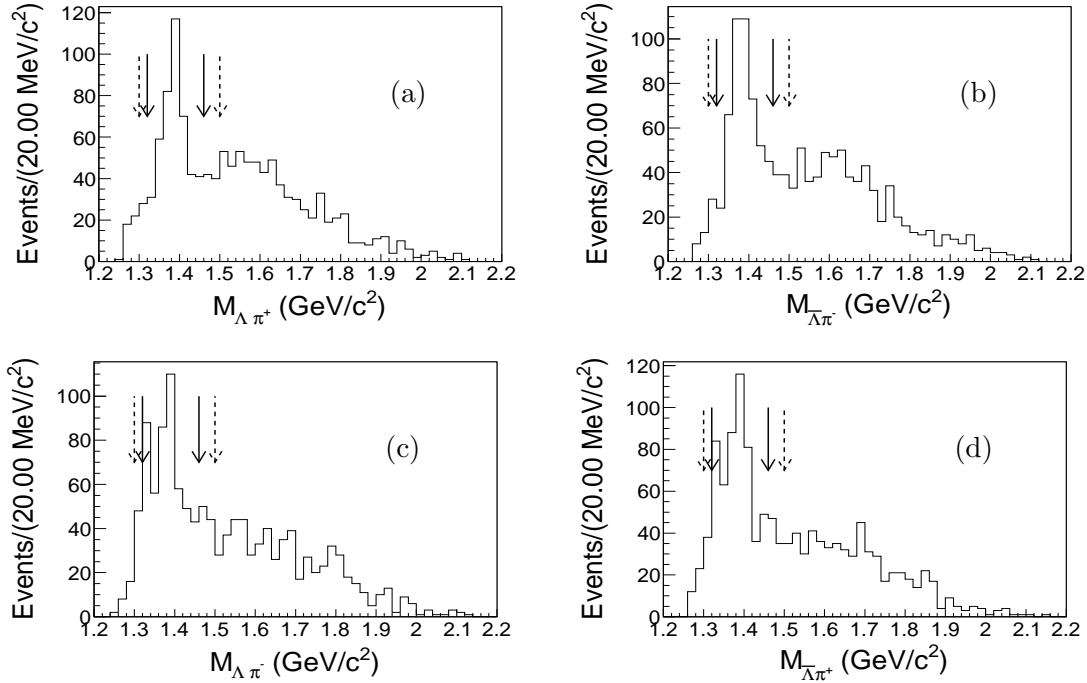
FIG. 2. The invariant mass distributions of (a) $\Lambda\pi^+$, (b) $\bar{\Lambda}\pi^-$, (c) $\Lambda\pi^-$ and (d)$\bar{\Lambda}\pi^+$. The areas between the two solid arrows are taken as the $\Sigma(1385)$ signal regions, while the areas outside the two dashed arrows are non-$\Sigma(1385)$ regions. The peaks of $\Xi^{\pm}$ in (c) and (d) will be rejected with the requirement $M_{\Lambda\pi^-(\bar{\Lambda}\pi^+)} > 1.331\,\mathrm{GeV}/c^2$ or $M_{\Lambda\pi^-(\bar{\Lambda}\pi^+)} < 1.312\,\mathrm{GeV}/c^2$.

into the above five processes cannot be completely separated using invariant mass regions alone. In this study, we separate the data into five independent categories, with dataset labels dataset-j ($j = 1, \cdots, 5$) defined as follows:

(i) dataset-1: the category to detect the non-resonant process 1. That is, events with $M_{\Lambda\pi^+}$, $M_{\bar{\Lambda}\pi^-}$, $M_{\Lambda\pi^-}$ and $M_{\bar{\Lambda}\pi^+}$ all in non-$\Sigma(1385)$ regions. The invariant mass spectrum of $\Lambda\bar{\Lambda}\pi^+\pi^-$ is displayed in Fig. 3 (a);

(ii) dataset-2: the category to detect the single resonant $\Sigma(1385)^+(\bar{\Sigma}(1385)^-)$ process 2. That is, events with $M_{\Lambda\pi^+}/M_{\bar{\Lambda}\pi^-}$ in the $\Sigma(1385)$ signal region and with $M_{\bar{\Lambda}\pi^-}(M_{\Lambda\pi^+})$, $M_{\Lambda\pi^-}$, $M_{\bar{\Lambda}\pi^+}$ in non-$\Sigma(1385)$ regions are required. The two types of events in this category are combined and displayed in Fig. 3 (b);

(iii) dataset-3: the category to detect the single resonant $\Sigma(1385)^-(\bar{\Sigma}(1385)^+)$ process 3. Similarly, events with $M_{\Lambda\pi^-}/M_{\bar{\Lambda}\pi^+}$ in $\Sigma(1385)$ signal region and with $M_{\bar{\Lambda}\pi^+}(M_{\Lambda\pi^-})$,

TABLE I. The number of fitted χ_{cJ} events in each dataset-j ($j = 1, \cdots, 5$) and the total dataset. n_j is the number of fitted χ_{cJ} events in dataset-j. n_{tot} is that in the total data sample.

Number of events	χ_{c0}	χ_{c1}	χ_{c2}
n_1	10.8 ± 3.8	12.7 ± 3.9	36.4 ± 6.4
n_2	36.4 ± 6.7	14.7 ± 4.1	47.6 ± 7.2
n_3	30.9 ± 6.6	12.5 ± 4.1	54.4 ± 7.9
n_4	27.4 ± 5.9	7.6 ± 3.2	14.6 ± 4.0
n_5	32.8 ± 6.3	3.6 ± 2.2	8.7 ± 3.3
n_{tot}	426 ± 23	105 ± 11	371 ± 20

$M_{\Lambda \pi^+}$, $M_{\bar{\Lambda} \pi^-}$ in non-$\Sigma(1385)$ regions are required. The two types of events in this category are combined and displayed in Fig. 3 (c);

(iv) dataset-4: the category to detect process 4. Events with $M_{\Lambda \pi^+}$, $M_{\bar{\Lambda} \pi^-}$ in $\Sigma(1385)$ signal region and $M_{\Lambda \pi^-}$, $M_{\bar{\Lambda} \pi^+}$ in non-$\Sigma(1385)$ region are selected and displayed in Fig. 3 (d);

(v) dataset-5: the category to detect process 5. Events with $M_{\Lambda \pi^-}$, $M_{\bar{\Lambda} \pi^+}$ in $\Sigma(1385)$ signal region and with $M_{\Lambda \pi^+}$, $M_{\bar{\Lambda} \pi^-}$ in non-$\Sigma(1385)$ region are selected and displayed in Fig. 3 (e).

The yield in each dataset is estimated by a fit to the χ_{cJ} peaks, and the yields of each process in the full phase space will be disentangled with Eq. (1), as described in Sec. V B.

The χ_{cJ} signal events are clearly observed in each category, as shown in Fig. 3 (a)–(e). In the fits of the χ_{cJ} in each dataset category, a Breit-Wigner function convolved with a Gaussian resolution function is used to describe χ_{cJ} peaks, while a 1st-order polynomial line is used to model the background distribution. The χ_{cJ} invariant mass parameters are allowed to float, while the χ_{cJ} widths are fixed to the PDG values [2]. The Gaussian parameters are obtained from MC simulation of detector responses. A simultaneous unbinned maximum likelihood method is applied, and the fit results are listed in Table I.
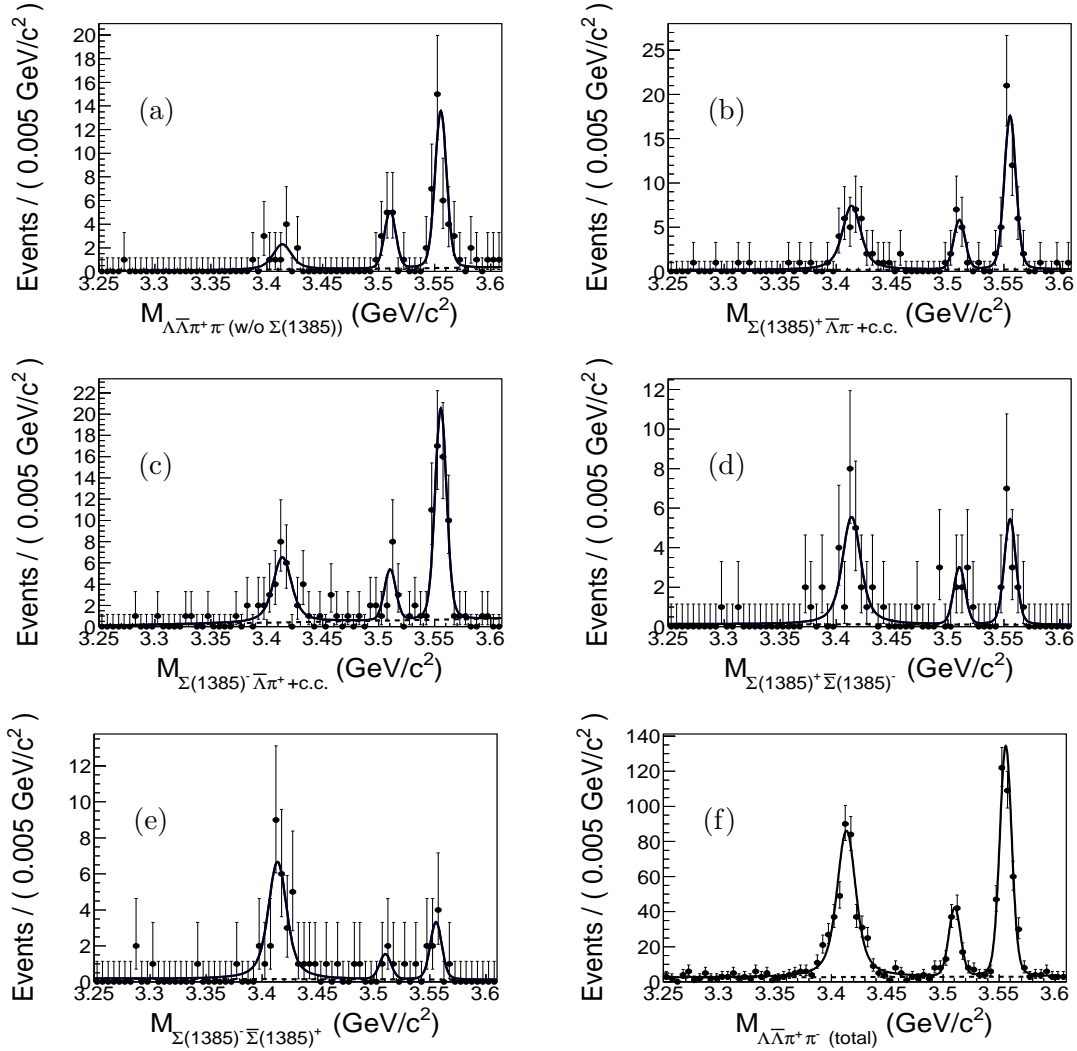
FIG. 3. The invariant mass distributions of $\Lambda\bar{\Lambda}\pi^+\pi^-$ in the following data samples: (a) dataset-1, (b) dataset-2, (c) dataset-3, (d) dataset-4, (e) dataset-5 and (f) total dataset. The selections of dataset-j ($j = 1, \cdots 5$) are defined in Sec. V. Points with error bars are data. The solid curves show the sum of the fitted curves, while the dashed lines are the backgrounds.

A. Background Study

A 106 million inclusive ψ'-decay MC sample is used to investigate possible ψ' decay backgrounds. No peaking backgrounds are observed, as shown in Fig. 1(d). Since a large proportion of the χ_{cJ} decays are poorly known and their simulations based on the BESIII LundCharm model have large uncertainty, we investigate possible underestimated peaking

backgrounds beneath the χ_{cJ} peaks. One major source could be from $\chi_{cJ} \to \Lambda K^{*+}\bar{p} \to$ $p\bar{p}\pi^+\pi^- K_s^0 \to p\bar{p}2\pi^+2\pi^-$ $(c.c.)$; however, the π^+ and π^- invariant mass distributions of candidate events were examined, and no evidence of a K_s peak was found. Therefore, negligible peaking background is assumed in this study. A study of the continuum data did not reveal any non-ψ' decay backgrounds.

B. Calculation of Branching Ratios

To calculate the branching ratios of each mode in $\chi_{cJ} \to \Lambda\bar{\Lambda}\pi^+\pi^-$ decay, one has to compute the efficiency-corrected number of χ_{cJ} decays. The numbers of χ_{cJ} events in dataset-j, which is selected to detect process i, also consists of events from the other processes. We describe the number of events of process i in dataset-j as

$$
\begin{pmatrix}
\varepsilon_{11} & \varepsilon_{12} & \varepsilon_{13} & \varepsilon_{14} & \varepsilon_{15} \\
\varepsilon_{21} & \varepsilon_{22} & \varepsilon_{23} & \varepsilon_{24} & \varepsilon_{25} \\
\varepsilon_{31} & \varepsilon_{32} & \varepsilon_{33} & \varepsilon_{34} & \varepsilon_{35} \\
\varepsilon_{41} & \varepsilon_{42} & \varepsilon_{43} & \varepsilon_{44} & \varepsilon_{45} \\
\varepsilon_{51} & \varepsilon_{52} & \varepsilon_{53} & \varepsilon_{54} & \varepsilon_{55}
\end{pmatrix}
\begin{pmatrix}
N_1 \\ N_2 \\ N_3 \\ N_4 \\ N_5
\end{pmatrix}
=
\begin{pmatrix}
n_1 \\ n_2 \\ n_3 \\ n_4 \\ n_5
\end{pmatrix},
\tag{1}
$$

where N_i is the efficiency-corrected number of events of process i, n_j are the numbers of χ_{cJ} events in the dataset-j (as listed in Table I), and ε_{ji} denotes the efficiency of process i being selected in dataset-j, obtained with MC simulation. In practice, the χ_{cJ} signals are fitted in the five datasets simultaneously, and with the constraint of the three efficiency matrices, N_1 – N_5 are obtained by the fit. Equations (2)–(4) are used to calculate branching ratios ($\mathcal{B}$) of the signal processes, and the results are listed in Table III. The significance of each decay mode, which is estimated using Eq. (5), is listed in Table III. Here L_m is the likelihood of the simultaneous fit, while $L_{m(N_j=0)}$ is the likelihood of the fit with the assumption that N_j is equal to zero.

$$
\mathcal{B}(\chi_{cJ} \to \Lambda\bar{\Lambda}\pi^+\pi^-(\text{non}-\text{resonant})) = \frac{N_1}{N_{\psi'}\mathcal{B}(\psi' \to \gamma\chi_{cJ})\mathcal{B}(\Lambda \to p\pi)^2}
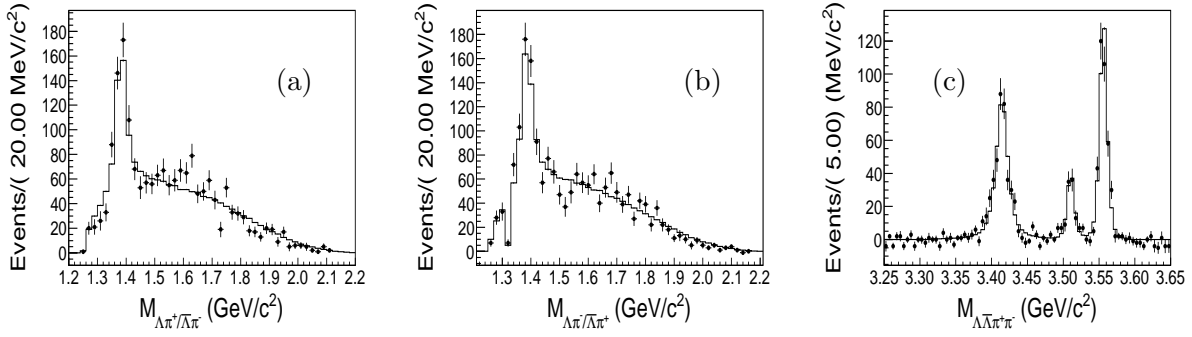\tag{2}
$$

FIG. 4. The invariant mass distributions of (a) $\Lambda\pi^+/\bar{\Lambda}\pi^-$, (b) $\Lambda\pi^-/\bar{\Lambda}\pi^+$ and (c) $\Lambda\bar{\Lambda}\pi^+\pi^-$. Points with error bars are the data with subtraction of the backgrounds, while solid lines are the MC simulation of the signals; The backgrounds subtracted are estimated from inclusive MC. The signal components are scaled based on their branching ratios measured in this work. The data within $1.312\,\mathrm{GeV}/c^2 < M_{\Lambda\pi^-(\bar{\Lambda}\pi^+)} < 1.331\,\mathrm{GeV}/c^2$ are removed to reject the $\Xi^\pm$ candidates.

$$\mathcal{B}(\chi_{cJ} \to \Sigma(1385)^{+(-)}\bar{\Lambda}\pi^{-(+)} + c.c.) = \frac{N_{2(3)}}{N_{\psi'}\mathcal{B}(\psi' \to \gamma\chi_{cJ})\mathcal{B}(\Sigma(1385) \to \Lambda\pi)} \cdot \frac{1.0}{\mathcal{B}(\Lambda \to p\pi)^2} \tag{3}$$

$$\mathcal{B}(\chi_{cJ} \to \Sigma(1385)^{+(-)}\bar{\Sigma}(1385)^{-(+)}) = \frac{N_{4(5)}}{N_{\psi'}\mathcal{B}(\psi' \to \gamma\chi_{cJ})\mathcal{B}(\Sigma(1385) \to \Lambda\pi)^2} \cdot \frac{1.0}{\mathcal{B}(\Lambda \to p\pi)^2} \tag{4}$$

$$S_j = \sqrt{2 \times (\ln L_m - \ln L_{m(N_j=0)})} \tag{5}$$

As shown in Fig. 4, the sum of measured components in the decays of χ_{cJ} into the final states $\Lambda\bar{\Lambda}\pi^+\pi^-$ in MC simulation agrees well with the data. This supports the credibility of the decomposition into the different components described above.

C. $\chi_{cJ} \to \Lambda\bar{\Lambda}\pi^+\pi^-$ (total)

Based on the selection criteria in Sec. IV, the process $\chi_{cJ} \to \Lambda\bar{\Lambda}\pi^+\pi^-$ (total), including the intermediate-resonant processes, is studied. The $\Lambda\bar{\Lambda}\pi^+\pi^-$ invariant mass distributions and the fit are displayed in Fig. 3 (f), while the fit results are listed in Table I. According to the measured branching ratios of the intermediate resonances in this analysis, signal MC

TABLE II. Sources of systematic uncertainties.

Sources	Relative systematic uncertainty (%)		
	χ_{c0}	χ_{c1}	χ_{c2}
$\Lambda\bar{\Lambda}$ reconstruction	3.5	3.5	3.5
$\pi^{\pm}$ tracking (not from $\Lambda\bar{\Lambda}$)	2.0	2.0	2.0
photon detection	1.0	1.0	1.0
kinematic fitting	1.0	1.0	1.0
vetoing background	4.9	2.6	4.4
fitting method	4.9	10.1	7.9
the number of ψ'	4.0	4.0	4.0
$\mathcal{B}(\psi' \to \gamma\chi_{cJ})$	3.2	4.3	4.0
$\mathcal{B}(\Sigma(1385)^{\pm} \to \Lambda\pi^{\pm})$	1.7	1.7	1.7
$\mathcal{B}(\bar{\Sigma}(1385)^{\mp} \to \bar{\Lambda}\pi^{\mp})$	1.7	1.7	1.7
total	9.6	12.7	11.4

samples are generated. This makes the momentum distributions of the final particles in the MC sample similar to those in experimental data and allows the determination of the overall detection efficiency, ε_{tot}, of the sum of all the processes with the same final states $\psi' \to \gamma\chi_{cJ} \to \gamma\Lambda\bar{\Lambda}\pi^{+}\pi^{-}$. The branching ratio of $\chi_{cJ} \to \Lambda\bar{\Lambda}\pi^{+}\pi^{-}$ (total) is calculated with the formula

$$\mathcal{B}(\chi_{cJ} \to \Lambda\bar{\Lambda}\pi^{+}\pi^{-}(\text{total})) = \frac{n_{\text{tot}}}{\varepsilon_{\text{tot}} \cdot N_{\psi'}\mathcal{B}(\psi' \to \gamma\chi_{cJ})\mathcal{B}(\Lambda \to p\pi)^{2}} \qquad (6)$$

VI.   SYSTEMATIC UNCERTAINTY

The systematic uncertainties in this analysis are summarized in Table II. Sources of systematic uncertainty include $\Lambda/\bar{\Lambda}$ reconstruction, $\pi^{\pm}$ tracking, photon detection, four-momentum constraint kinematic fitting, background rejection, χ_{cJ} signal fitting, the number of ψ' events and branching ratios cited from the PDG [2]. Charged π tracking and photon detection systematic errors are studied following the methods in Refs. [4, 5].

For the systematic uncertainty due to $\Lambda/\bar{\Lambda}$ reconstruction, $J/\psi \to \Lambda\bar{\Lambda}\pi^+\pi^-$ and $\psi' \to \pi^+\pi^- J/\psi \to \Lambda\bar{\Lambda}\pi^+\pi^-$ are used to select a $\Lambda/\bar{\Lambda}$ control sample. $\Lambda/\bar{\Lambda}$ reconstruction efficiency is calculated by taking the ratio of the fitted $\Lambda/\bar{\Lambda}$ yields in the missing mass spectrum before and after $\Lambda/\bar{\Lambda}$ is found. $\Lambda/\bar{\Lambda}$ reconstruction efficiencies consist of tracking efficiency of the daughter particles and the vertex-constraint of $\Lambda/\bar{\Lambda}$. The differences in the efficiencies between experimental data and the MC sample are included in the systematic uncertainties.

To study the efficiency of the kinematic fitting in the four-momentum constraint, event candidates for the three processes $\psi' \to \gamma\Lambda\bar{\Lambda}\pi^+\pi^-$, $\psi' \to \gamma\chi_{cJ} \to \gamma3(\pi^+\pi^-)$ and $\psi' \to J/\psi\pi^+\pi^- \to 3(\pi^+\pi^-)\pi^0 \to 3(\pi^+\pi^-)2\gamma$ are used as control samples. The ratio of the event rates before and after the kinematic fitting is taken as the efficiency of the kinematic fitting. These efficiencies are calculated both in experimental data and in the MC sample, and their difference determines the uncertainty of the kinematic fitting.

For the rejection of the resonances J/ψ, $\Sigma^0/\bar{\Sigma}^0$ and $\Xi^\pm$, different J/ψ, Σ^0, $\bar{\Sigma}^0$ and $\Xi^\pm$ mass region requirements are applied ranging from 3σ, 3.5σ to 4σ, where σ is the detector resolution. The largest deviation on the branching ratios is taken as the systematic uncertainty. The systematic uncertainty of the fitting method is obtained by changing the fitting range, the shape of the backgrounds, and changing the detector resolution from the value obtained with MC simulation to that obtained by fitting with a free parameter. The relative uncertainty of the estimated number of ψ' is 4.0% [4]. The uncertainty of the branching ratios of intermediate decays are taken from the PDG [2]. The total systematic uncertainty is obtained by summing all the individual uncertainties in quadrature.

VII. RESULTS AND DISCUSSION

The branching ratios of χ_{cJ} decays to $\Sigma(1385)^\pm\bar{\Sigma}(1385)^\mp$, $\Sigma(1385)^\pm\bar{\Lambda}\pi^\mp + c.c.$ and $\Lambda\bar{\Lambda}\pi^+\pi^-$ (with or without the $\Sigma(1385)$ resonance) are measured with 106 million ψ' decay events collected at BESIII. The results are listed in Table III. The process $\chi_{cJ} \to \Lambda\bar{\Lambda}\pi^+\pi^-$ is observed for the first time. Evidence of $\chi_{c0} \to \Sigma(1385)^\pm\bar{\Sigma}(1385)^\mp$, which strongly violates the helicity selection rule, is presented. The branching ratios of $\chi_{c1,2} \to \Sigma(1385)^\pm\bar{\Sigma}(1385)^\mp$ are consistent with the theoretical predictions [1].

TABLE III. Results of the branching ratios ($\times 10^{-5}$) for different decay modes. 'UL' stands for the upper limit of the branching ratio at the 90% C.L. 'S' stands for the statistical significance. The first errors are statistical and the second systematic.

χ_{cJ} decay mode	χ_{c0}			χ_{c1}			χ_{c2}		
	$\mathcal{B}$	UL	S	$\mathcal{B}$	UL	S	$\mathcal{B}$	UL	S
$\Lambda\bar{\Lambda}\pi^+\pi^-$ (w/o $\Sigma(1385)$)	28.6±12.6±2.7	<54	2.2	26.2±5.5±3.3		4.8	71.8±14.5±8.2		6.4
$\Sigma(1385)^+\bar{\Lambda}\pi^- + c.c.$	34.8±13.2±3.4	<55	2.2		<14	0.3	23.6±11.8±2.7	<42	1.7
$\Sigma(1385)^-\bar{\Lambda}\pi^+ + c.c.$	24.6±12.7±2.4	<50	1.6		<14	0.0	37.8±11.8±4.4	<61	2.6
$\Sigma(1385)^+\bar{\Sigma}(1385)^-$	16.4±5.7±1.6		3.1	4.4±2.5±0.6	<10	1.9	7.9±4.0±0.9	<17	2.0
$\Sigma(1385)^-\bar{\Sigma}(1385)^+$	23.5±6.2±2.3		4.3		<5.7	0.9		<8.5	0.0
$\Lambda\bar{\Lambda}\pi^+\pi^-$(total)	119.0±6.4±11.4		> 10	31.1±3.4±3.9		> 10	137.0±7.6±15.7		> 10

VIII. ACKNOWLEDGMENTS

R32-2008-000-10155-0.

[1] S.M. Wong, Nucl. Phys. A **674**,185 (2000).

[2] J. Beringer *et al.* (Particle Data Group), Phys. Rev. D **86**, 010001 (2012).

[3] S. J. Brodsky and G. P. Lepage, Phys. Rev. D **24**, 2848 (1981).

[4] M. Ablikim *et al.* (BESIII Collaboration), Phys. Rev. D **81**, 052005 (2010).

[5] M. Ablikim *et al.* (BESIII Collaboration), Nucl. Instrum. Meth. A **614**, 345 (2010).

[6] S. Jadach, B.F.L. Ward and Z. Was, Comp. Phys. Commu. **130**, 260 (2000).

[7] S. Jadach, B.F.L. Ward and Z. Was, Phys. Rev. D **63**, 113009 (2001).

[8] K. -T. Chao *et al.*, Modern physics A, **24** No.1 supp. (2009).

[9] R. G. Ping, Chin. Phys. C **32**, 599 (2008).

[10] G. Karl *et al.*, Phys. Rev. D **13**, 1203 (1976); P. K. Kabir and A. J. G. Hey, Phys. Rev. D **13**, 3161 (1976).